Journal of Catalysis 279 (2011) 36–47

Contents lists available at ScienceDirect

Journal of Catalysis

journal homepage: www.elsevier.com/locate/jcat

Structure sensitivity of dodecahydro-N-ethylcarbazole dehydrogenation over Pd catalysts

Farnaz Sotoodeh, Kevin J. Smith *

Department of Chemical & Biological Engineering, University of British Columbia, 2360 East Mall, Vancouver, BC, Canada V6T 1Z3

ARTICLE INFO

Article history:
Received 8 November 2010
Revised 29 December 2010
Accepted 30 December 2010

Keywords:
Dehydrogenation
Kinetics
Catalyst
Pd/SiO_2
Dodecahydro-N-ethylcarbazole (perhydro-N-ethylcarbazole)
N-ethylcarbazole
Hydrogen storage and recovery
DFT

ABSTRACT

The complete recovery of the H_2 stored on dodecahydro-N-ethylcarbazole was achieved at 443 K and 101 kPa using Pd/SiO_2 catalysts, prepared by incipient wetness impregnation with calcination in He rather than air. The dehydrogenation turn-over frequency (TOF) and selectivity to the completely dehydrogenated product, N-ethylcarbazole, were dependent upon Pd particle size, with a maximum in both occurring with a 4 wt.% Pd/SiO_2 catalyst that had an average Pd particle size of 9 nm. Over this catalyst, the dehydrogenation reaction proceeded to complete conversion within 22 min and complete H_2 recovery (5.8 wt.%) within 1.6 h at 443 K and 101 kPa. The structure sensitivity of the reaction and the observed product distribution are discussed in view of DFT calculations that showed that the adsorption of dodecahydro-N-ethylcarbazole on Pd required multiple catalytic sites and the heat of adsorption was dependent upon the surface structure.

1. Introduction

Hydrogen is an alternative, non-toxic, environmentally benign energy carrier with H_2O the only product when H_2 is converted into thermal energy (by combustion) or electrical energy (using fuel cells). However, hydrogen has a very low density at ambient conditions making it difficult to store and transport. On-board vehicular hydrogen storage, including compressed or liquid (cryogenic) hydrogen, suffers from high-energy inputs and low gravimetric storage capacities. On the other hand, organic aromatic compounds that bind hydrogen covalently have the potential to meet the 6 wt.% H_2 storage density demands of automotive applications [1].

Storage and release of hydrogen from organic compounds is achieved by catalytic hydrogenation and dehydrogenation reactions, respectively. The dehydrogenation reaction must be fast, selective and have low enthalpy so that the reaction is thermodynamically favored at low temperature (<473 K) [2]. However, a review of literature data shows very slow dehydrogenation reaction rates and low selectivity to the completely dehydrogenated product for some organic compounds. For example, the high enthalpy of dehydrogenation of cyclohexane (205.5 kJ/mol with H_2 capacity 7.1 wt.%) and methylcyclohexane (202.5 kJ/mol with H_2 capacity 6.1 wt.%) means that high temperatures (>573 K) are required for on-board H_2 recovery by dehydrogenation [3–5]. Pez et al. [6] have shown that incorporation of a heteroatom in the aromatic ring can lower the dehydrogenation enthalpy of the candidate compounds. Complete conversion of indoline, with a hydrogen capacity of 1.7 wt.%, was reported over Pd/C and Rh/C catalysts after 24 h in refluxing toluene (~383 K) [7]. However, the low hydrogen content of indoline means that this is not a practical choice for transport applications. Dehydrogenation of 4-aminopiperidine (hydrogen capacity 5.9 wt.%) over a 10 wt.% Pd/SiO_2 catalyst resulted in 66% conversion at 443 K after 4 h [2]. Complete conversion of dodecahydro-N-ethylcarbazole (hydrogen capacity 5.8 wt.%) was obtained over a 5 wt.% Pd/SiO_2 at 443 K and 101 kPa after 17 h with only 4.0 wt.% H_2 recovery, due to a low selectivity toward the completely dehydrogenated N-ethylcarbazole product [8,9]. Dehydrogenation of dodecahydrocarbazole (hydrogen capacity 6.7 wt.%) was reported to be even slower than dodecahydro-N-ethylcarbazole, most likely due to product inhibition by carbazole, where only 53% conversion was achieved after 17 h at 443 K and 101 kPa [8,9]. In a similar dehydrogenation study of dodecahydro-N-ethylcarbazole over homogeneous Ir-complex catalysts, no selectivity toward N-ethylcarbazole was reported at 473 K, and octahydro-N-ethylcarbazole and tetrahydro-N-ethylcarbazole were the only products [10].

* Corresponding author.
E-mail address: kjs@interchange.ubc.ca (K.J. Smith).

0021-9517/$ - see front matter © 2011 Elsevier Inc. All rights reserved.
doi:10.1016/j.jcat.2010.12.022

Despite reports of low activity and selectivity to the completely dehydrogenated products, limited data are available on the relationship between catalytic activity and catalyst dispersion for the hydrogenation and dehydrogenation reactions of organic aromatics, and contradictory interpretations have been reported. For example, Benedetti et al. [11] reported that the hydrogenation of 2,4-dinitrotoluene over Pd/SiO_2 was favored by an increase in Pd particle size. However, Suh et al. [12] noted that hydrogenation of 2,4-dinitrotoluene over Pd/C catalysts was structure insensitive and that increases in specific activity on larger Pd particles was attributed to diffusion limitations within the pores of the microporous carbon support. In other work on the hydrogenation of 2,4-dinitrotoluene over a Pd/C catalyst, it was found that in the range of dispersions investigated (Pd particle size 3–10 nm), the specific activities increased as the Pd dispersion decreased [13]. In a study of pyrrole hydrogenation over Pt catalysts, with particle size from <1 nm to 5 nm, reported by Kuhn et al. [14], it was demonstrated that ring hydrogenation was structure insensitive, while ring opening to *n*-butylamine was structure sensitive and found to be more facile over larger Pt nanoparticles.

Adsorption geometries of aromatic organic compounds relevant to hydrogen storage over metal surfaces have been shown to involve several surface metal atoms, suggesting that the dehydrogenation reactions may be structure sensitive. Crawford et al. [15] investigated the mechanism of 1,2,3,4-tetrahydrocarbazole dehydrogenation over a Pd catalyst, and showed by experiment and density-functional theory (DFT) calculations that the reaction proceeded through a flat 1,2,3,4-tetrahydrocarbazole adsorption geometry involving several Pd surface sites. Lu et al. [16], using periodic DFT calculations, also reported a flat adsorption of tetracene over several Ru surface atoms, with the long axis of tetracene parallel to the surface. The optimized structure showed that adsorption of tetracene required multiple Ru atoms. Tilted and parallel adsorption of quinoline on a Pt cluster investigated by Vargas et al. [17] also indicated that several surface Pt atoms were involved in the adsorption.

In the present work, the structure sensitivity of the dehydrogenation of dodecahydro-N-ethylcarbazole was investigated over a series of Pd/SiO_2 catalysts, prepared with Pd loadings of 0.5–10 wt.%, such that the Pd dispersion (particle size) varied from 6.5% (15 nm) to 52% (1.9 nm). The activity and selectivity of each catalyst for the dehydrogenation of dodecahydro-N-ethylcarbazole is reported. DFT calculations, used to identify the initial H removal sites of the dodecahydro-N-ethylcarbazole molecule, are reported and used to rationalize the observed dehydrogenation product distribution.

2. Experimental

2.1. Catalyst Preparation

The SiO_2-supported Pd catalysts (0.5–10 wt.%) were prepared by incipient wetness of the support [18]. Silica gel (Sigma–Aldrich, BET surface area 400 m^2/g, pore volume 1.15 cm^3/g, particle size <90 μm) was used as the support. Approximately 10 g of the silica gel was drop-wise impregnated with an aqueous solution of Pd^{2+}, prepared from 0.5 N HCl and the $PdCl_2$ (Sigma–Aldrich, 99.9+%), at a concentration sufficient to yield the required Pd loading from one impregnation. The impregnated support was left to age for 48 h before being dried at 393 K for 8 h and calcined at 773 K for 6 h in a He flow of 30 cm^3 (STP)/min. The calcined catalyst precursor was subsequently reduced in a H_2 flow of 30 cm^3 (STP)/min while heating at a rate of 10 K/min to 673 K. The final temperature was held for 1 h before cooling the reduced catalyst to room temperature in a 30-cm^3 (STP)/min flow of He.

The Pd catalysts were compared to a previously reported 5 wt.% Pd/SiO_2 catalyst that was prepared by wet impregnation but dried at 393 K for 24 h and calcined at 748 K for 3 h in air rather than inert He [8]. Using the same procedure, a 10 wt.% Pd/SiO_2 catalyst calcined in air was also prepared in the present study.

2.2. Catalyst characterization

Temperature-programmed reduction (TPR) of the calcined Pd/SiO_2 catalyst precursors was performed using a Micromeritics Autochem II 2920 analyser fitted with a thermal conductivity detector (TCD). About 0.2 g of each sample was loaded into a u-tube reactor and flushed for 30 min in a 50-cm^3 (STP)/min flow of 10% H_2 in Ar at room temperature, before heating to 673 K at a rate of 10 K/min with the final temperature held for 1 h.

In order to clarify the TPR profiles, additional TPR studies were done using a quartz u-tube reactor placed in a temperature-programmable muffle furnace with a quadrupole mass spectrometer (SRC Residual Gas Analyzer, 200 amu) connected to the reactor effluent in order to continuously monitor the products generated during the temperature-programmed calcination and reduction. The calcination and reduction steps, using 0.4 g of sample, followed the same procedure as that used in the Micromeritics Autochem II 2920 analyser. To investigate the reducibility of the catalyst at room temperature, the catalysts were flushed in a 50-cm^3 (STP)/min flow of 10% H_2 in He for 3 h at room temperature after the calcination and prior to the TPR.

Temperature-programmed desorption (TPD) of CO from the Pd catalysts was also performed using the Micromeritics Autochem II 2920 analyser. About 0.2 g of the dried catalyst was loaded into the reactor and calcined at 773 K for 6 h in a flow of Ar at 30 cm^3 (STP)/min, followed by TPR at 10 K/min to a final temperature of 673 K in a 30-cm^3 (STP)/min flow of 10% H_2 in Ar, holding the final temperature for 1 h. The catalyst was then flushed in a 30-cm^3 (STP)/min flow of Ar for 1 h and cooled to room temperature, before being exposed to a 50-cm^3 (STP)/min flow of 10% CO in He at 313 K for 1 h. The catalyst was subsequently flushed in 50 cm^3 (STP)/min He for 2 h. The temperature-programmed desorption was then started in the same He flow by heating the sample to 773 K at a rate of 10 K/min and holding the final temperature for 1 h.

The catalysts were also characterized by high-resolution transmission electron microscopy (HRTEM), scanning electron microscopy (SEM), and energy dispersive X-ray analysis (EDX). SEM, EDX, and EDX-mapping were done using a variable pressure 120 keV Hitachi S-3000 N equipped with a light element EDX detector. A FEI Tecnai G2 200 keV with a LaB_6 filament capable of 1.4 Å point-to-point resolution was used for high-resolution transmission electron microscopy (HRTEM). Pd/SiO_2 samples with variable Pd loadings were ground to a fine powder using an agate mortar and pestle and dispersed in ethanol ultrasonically. A droplet of the suspension was then placed on a 200-mesh copper grid coated with formvar carbon and left to dry before analysis.

2.3. Catalyst activity

The dodecahydro-N-ethylcarbazole reactant was prepared by hydrogenation of N-ethylcarbazole at 423 K and a H_2 pressure of 7 MPa. A 300-cm^3 autoclave batch reactor with continuous monitoring and control of stirrer speed, temperature, and pressure was used for the hydrogenation reaction. Details of the experimental procedure and reactor set-up for the hydrogenation reaction have been reported elsewhere [8,9].

The dehydrogenation reactions were carried out in a 50-cm^3 glass flask reactor, operated in batch mode at 443 K and 101 kPa using the reduced Pd/SiO_2 catalysts. For each experiment, 10 cm^3

of the product recovered from N-ethylcarbazole hydrogenation was diluted in 20 cm^3 of decalin (Sigma–Aldrich, 98%) and added to the reactor as reactant of the dehydrogenation reaction. The reactor was stirred at 550 rpm and heated to the desired temperature while purging in He flow at 171 cm^3 (STP)/min. Once the reaction temperature was reached, the catalyst was injected into the reactor using a syringe. The He flow was maintained and acted as a carrier gas for continuous removal of the produced hydrogen. The reactor exit gas composition was continuously monitored using a quadrupole mass spectrometer (SRC Residual Gas Analyzer, 200 amu). Liquid samples of ~0.1 ml were withdrawn from the reactor periodically and analyzed using a Shimadzu QP-2010S GC/MS and a Restek RTX5 30 m × 0.25 mm capillary column. Internal mass transfer effects were minimal because of the small catalyst particle size (<90 μm) that resulted in a calculated Weisz–Prater parameter of $\Phi < 1.0$ at the reaction temperature.

2.4. DFT calculations

The DFT calculations were performed using DMol^3 [19,20] in Material Studio 4.4.0.0. (Accelrys Inc.). Double-numeric quality basis set (DNP) with the gradient-corrected GGA functional of Becke [21] and PBE description of exchange and correlation effects [22,23] were used to optimize the geometry of the molecules. A Fermi smearing of 2×10^{-3} Ha, a real-space cut-off of 4.0 Å and a MEDIUM quality mesh size (using about 1000 grid points for each atom in the calculation) was used for the numerical integration. The Pd(1 1 1) surface was created with a (3 × 3) supercell and four Pd layers with a 30-Å vacuum region between the slabs. Adsorption geometry of the molecule was obtained by allowing the molecule and the top layer of the Pd(1 1 1) surface to relax. Density functional semi-core pseudopotentials (DSPP) were used for the Pd substrate. The tolerances of energy, gradient, and displacement convergence were 2×10^{-5} Ha, 4×10^{-3} Ha/Å, and 5×10^{-3} Å, respectively. Adsorption energies were determined as $E_{adsorption} = E_{adsorbed\ molecule/surface} - E_{molecule\ in\ vacuum} - E_{surface}$, where $E_{adsorbed\ molecule/surface}$ is the energy of the adsorption system, $E_{molecule\ in\ vacuum}$ is the energy of the adsorbed molecule in vacuum, and $E_{surface}$ is the energy of the surface.

3. Results

3.1. Catalyst properties

Representative H_2 TPR profiles for the 0.5 wt.%, 10 wt.% He-calcined, and 10 wt.% air-calcined Pd/SiO_2 catalysts are presented in Fig. 1. Similar TPR profiles were observed for all the other Pd/SiO_2 He-calcined catalysts. A negative peak in all the TPR profiles, indicative of a net H_2 evolution from the sample rather than H_2 consumption, was observed at temperatures between 333 and 360 K. Babu et al. [24] reported very similar H_2 TPR profiles for 5 wt.% and 3 wt.% Pd/alumina catalysts, where H_2 evolution from the Pd in the region 348–373 K, was observed. In work by Amairia et al. [25], H_2 TPR profiles from Pd/Al_2O_3–ZrO_2 also showed H_2 evolution at 358 K. The H_2 profile is consistent with the release of H_2 from the decomposition of a β-palladium hydride phase which is reported to form at room temperature over large Pd particles (>2 nm) [11,13,24–27] and in the present work, was likely generated during the low temperature flush in 10% H_2 in He for 30 min that followed catalyst calcination.

Figs. 2 and 3 compare the effluent gas profiles as measured by mass spectrometer during the thermal treatment of the silica gel support and the catalyst precursors. The silica gel and the 10 wt.% Pd/SiO_2 precursor were calcined at 773 K in He (Fig. 2a and b, respectively) or air (Fig. 3a and b, respectively). The He-

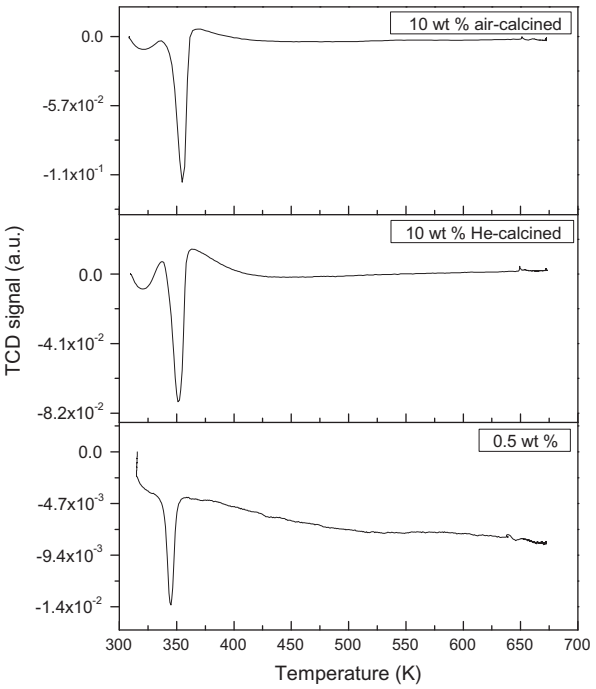

Fig. 1. Selected TPR patterns of SiO_2 supported Pd catalysts with different Pd loadings.

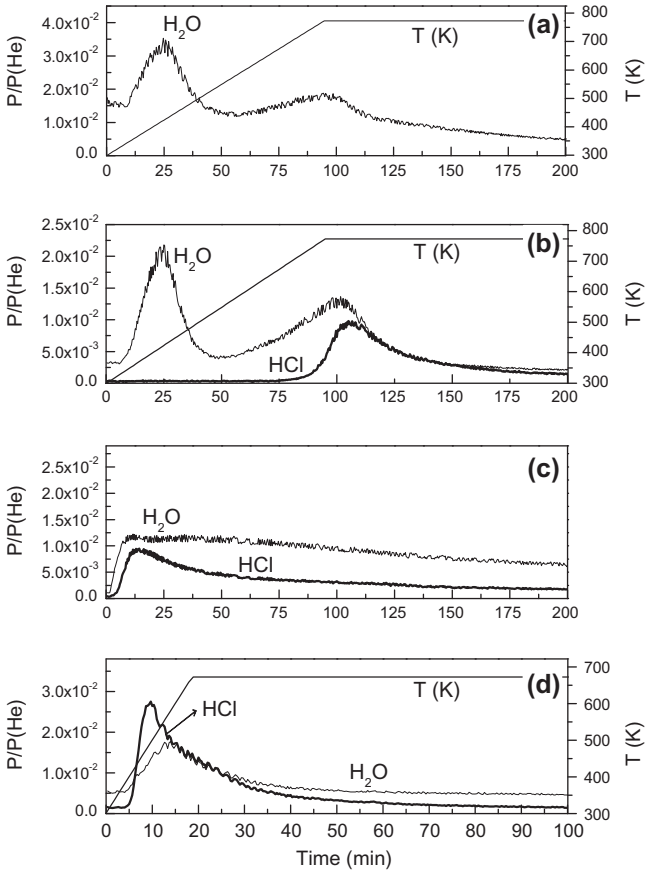

Fig. 2. Profile of effluent gases during thermal treatment of catalyst samples in He as measured by mass spectrometer using 0.4 g of sample. (a) SiO_2 gel calcination in He at 773 K, (b) 10 wt.% Pd/SiO_2 calcination in He at 773 K, (c) 10 wt.% Pd/SiO_2 flush in 10% H_2 in He at room temperature, and (d) 10 wt.% Pd/SiO_2 reduction in 10% H_2 in He at 673 K.

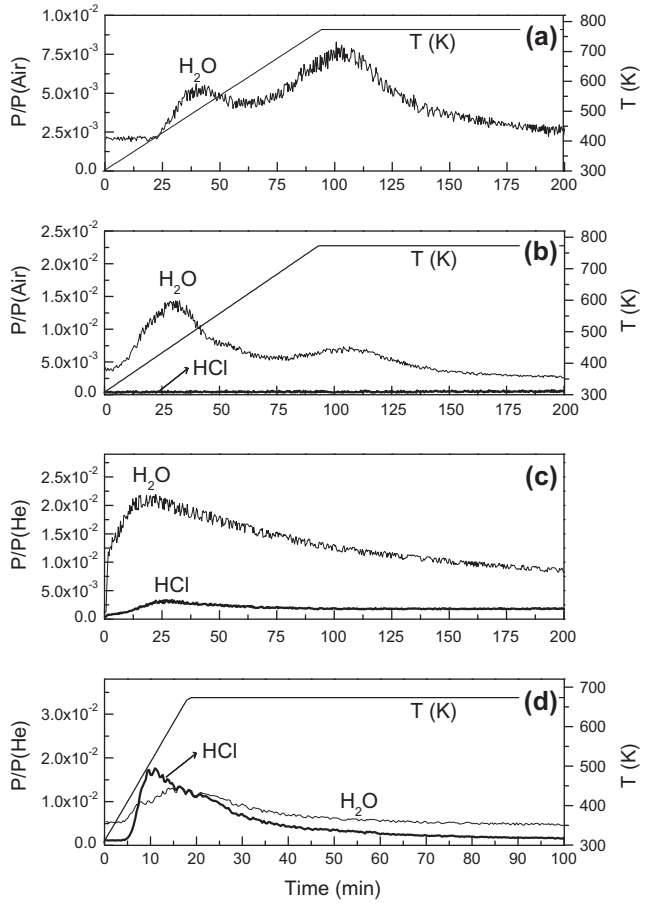

Fig. 3. Profile of effluent gases during thermal treatment of catalyst samples in air as measured by mass spectrometer using 0.4 g of sample. (a) SiO_2 gel calcination in air at 773 K, (b) 10 wt.% Pd/SiO_2 calcination in air at 773 K, (c) 10 wt.% Pd/SiO_2 flush in 10% H_2 in He at room temperature, and (d) 10 wt.% Pd/SiO_2 reduction in 10% H_2 in He at 673 K.

calcined and the air-calcined 10 wt.% Pd/SiO_2 catalyst precursors were then flushed in 10% H_2 in He at room temperature (Figs. 2c and 3c) and reduced in the same flow of gas by temperature programming to 673 K at 10 K/min (Figs. 2d and 3d). Calcination of the silica gel in He (Fig. 2a) resulted in the production of two water peaks at about 425 K and 773 K. The two water peaks were also observed during the calcination of the silica gel in air at approximately 500 K and 773 K (Fig. 3a). Comparing the calcination of the Pd/SiO_2 in He or air (Figs. 2b and 3b, respectively) shows that a sharp peak between 423 and 500 K and a second broader peak at 773 K for water evolution were observed for both samples. HCl evolution was also detected for the catalyst calcined in He with a peak temperature at 773 K (Fig. 2b), whereas no HCl was observed for the sample calcined in air (Fig. 3b). Subsequent flushing of the catalysts in a flow of 10% H_2 in He at room temperature resulted in the production of water and HCl from both catalysts, with more HCl observed for the catalyst calcined in He (Fig. 2c) compared to the one calcined in air (Fig. 3c). The catalyst flush steps were followed by TPR in a flow of 10% H_2 in He at 20 K/min to 673 K which revealed a significant production of HCl (especially for the catalyst calcined in He) as well as water. For the Pd/SiO_2 calcined in He, the peak in water evolution occurred at 488 K and the peak in HCl evolution occurred at 578 K (Fig. 2d). For the air-calcined sample, the corresponding peak temperatures were 520 K and 620 K, respectively (Fig. 3d).

Table 1 summarizes the properties of the catalysts prepared in the present study (i.e. 0.5–10 wt.% Pd/SiO_2 prepared by calcination in He and the 10 wt.% Pd/SiO_2 catalyst prepared by calcination in air), and the 5 wt.% Pd/SiO_2 catalyst prepared by wet impregnation and calcination in air, reported by Sotoodeh et al. [8]. Fig. 4 shows the results obtained from the temperature-programmed desorption (TPD) of CO from the 0.5, 4, and 10 wt.% Pd/SiO_2 catalysts. Similar profiles were observed for the other He-calcined Pd/SiO_2 catalysts. The major desorption peak occurred at 343–362 K, in good agreement with the desorption peak temperature of 320–350 K reported by Myyrylainen et al. [28] for the TPD of CO from a Pd(1 0 0) surface. The CO uptake determined from the TPD experiments was used to estimate the catalyst dispersion at each Pd loading, as well as the Pd particle diameter, assuming a CO:Pd adsorption stoichiometry of 1:1 [29]. The results, summarized in Table 1, show that the Pd particle size of the Pd/SiO_2 catalysts varied from 2 to 15 nm as the Pd loading increased from 0.5 wt.% to 10 wt.%. By comparing these results to the 10 wt.% and the 5 wt.% Pd/SiO_2 [8,9] catalysts calcined in air and shown in Table 1, it is clear that a significant increase in the dispersion of the Pd catalysts was obtained by calcination in He rather than air. The particle size decreased from 27.9 nm to 15.4 nm for the 10 wt.% Pd/SiO_2 by calcining the catalyst in He rather than air. The 5 wt.% Pd/SiO_2 calcined in He had a Pd metal dispersion of 7.9%, almost twice the value of 4.2% obtained for the 5 wt.% Pd/SiO_2 catalyst prepared by calcination in air [8,9].

The reduced and calcined Pd/SiO_2 samples were analyzed by SEM and EDX to investigate the catalyst morphology, as well as the elemental composition. Table 2 summarizes the EDX elemental analysis of the 5 wt.% Pd/SiO_2 catalysts, reported as the average of at least 10 point analyses, after various thermal treatments. Calcination in He or air at 773 K for 6 h did not remove all the Cl present in the precursor and Cl was identified after calcination in He or air. However, as shown in Table 2, no Cl was present after TPR of the sample calcined in He, whereas a small amount of Cl was detected after the TPR of the sample calcined in air.

Further insight into the size distribution of the Pd/SiO_2 catalysts was obtained by high-resolution transmission electron microscopy (HRTEM) of the reduced Pd/SiO_2 catalysts as summarized in Table 1. Fig. 5a–c shows selected HRTEM images of the reduced 10 wt.%, 4 wt.%, and 0.5 wt.% Pd/SiO_2 catalysts, respectively. The Pd size distribution obtained from several HRTEM images were fitted to a log-normal distribution to obtain an estimate of the average Pd particle diameter and standard deviation with Pd loading. The results, reported in Table 1, showed good agreement with the values calculated from the CO TPD data.

Table 1
Properties of reduced Pd/SiO_2 catalysts with Pd loading of 0.5–10 wt.%, obtained by TPD of CO and HRTEM. All catalysts calcined in He unless otherwise stated.

Pd loading (wt.%)	CO desorbed (μmol/g)	Dispersion (%)	Pd particle size[c] (nm)	Average Pd particle diameter (nm)
0.5	20.9	51.9	1.9	3.6[d] ± 0.1[e]
0.7	25.3	44.7	2.2	4.0 ± 0.2
1	22.5	28.3	3.6	4.6 ± 0.2
2	25.7	16.0	6.3	6.1 ± 0.1
3	31.0	12.9	7.7	7.0 ± 0.1
4	34.4	11.0	9.1	7.3 ± 0.4
5	30.3	7.9	12.5	13.2 ± 0.9
10	53.1	6.5	15.4	15.5 ± 0.7
10[a]	–	3.6[b]	27.9[b]	23.7 ± 2.7
5[a]	–	4.2[b]	23.8[b]	–

[a] Reduced after calcination in air.
[b] Obtained by CO pulse chemisorption.
[c] Obtained from CO TPD analysis.
[d] Average Pd particle size obtained by fitting HRTEM data to a log-normal distribution.
[e] Standard deviation of average particle size obtained from the log-normal fit.

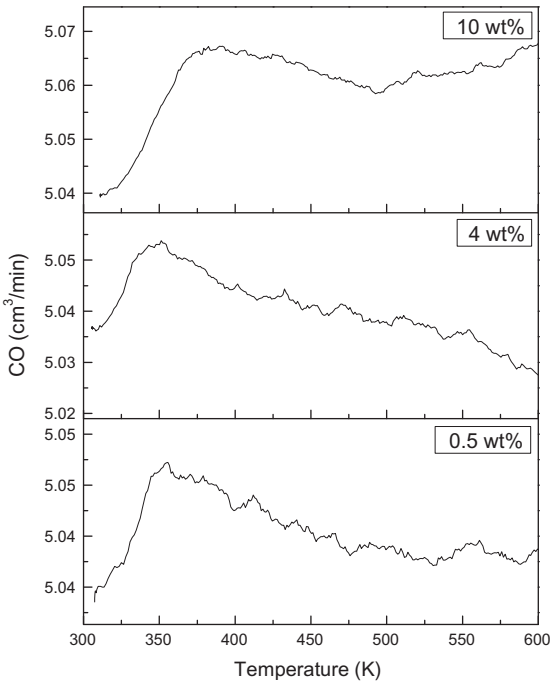

Fig. 4. Selected temperature-programmed desorption (TPD) of CO from Pd/SiO_2 catalysts with different Pd loadings at a heating rate 10 K/min.

Table 2
EDX elemental analysis of the 5 wt.% Pd/SiO_2 catalysts.

Status	Reduced after He calcination	Reduced after air calcination	Calcined in He	Calcined in air
Element	Concentration (wt.%)			
Oxygen	56.3 ± 3.1	57.8 ± 0.2	52.4 ± 0.4	57.6 ± 0.3
Silicon	38.6 ± 1.9	35.9 ± 0.2	37.9 ± 1.3	37.7 ± 0.1
Chlorine	0.00 ± 0.00	0.03 ± 0.01	0.8 ± 0.1	1.0 ± 0.1
Palladium	5.1 ± 1.9	6.2 ± 0.1	8.8 ± 1.2	3.7 ± 0.2

3.2. Catalyst activities

Dehydrogenation of the dodecahydro-N-ethylcarbzole was carried out over each of the reduced Pd/SiO_2 catalysts. The reactor was operated at 443 K and 101 kPa. Decalin was used as the solvent in the dehydrogenation reaction. The stability of decalin at reaction temperatures below 473 K over Pd/SiO_2 catalysts has been confirmed in previous studies [8,30–33]. Figs. 6–8 show the product distribution as a function of reaction time obtained from the GC/MS liquid sample analysis of the dehydrogenation products. The data show that octahydro-N-ethylcarbazole and tetrahydro-N-ethylcarbazole were the primary products of the reaction, and the reactions proceeded with further conversion of these two intermediates and the production of the completely dehydrogenated product, N-ethylcarbazole, according to the following stoichiometry:

$$C_{14}H_{25}N \rightarrow C_{14}H_{21}N + 2H_2$$

$$C_{14}H_{21}N \rightarrow C_{14}H_{17}N + 2H_2$$

$$C_{14}H_{17}N \rightarrow C_{14}H_{13}N + 2H_2$$

Comparing the product distributions in Figs. 6–8 as a function of the catalyst Pd loading, it is clear that the same intermediates and products were identified for each catalyst. However, the product selectivity was dependent upon the Pd loading and hence the Pd particle size, and in no case was hexahydro-N-ethylcarbazole nor decahydro-N-ethylcarbazole (two other possible hydrogenation reaction intermediates) observed. More importantly, the catalysts prepared by calcination in He were remarkably selective to the completely dehydrogenated compound, N-ethylcarbazole. As shown by the data of Figs. 6 and 7, increased Pd loading from 0.5 to 4 wt.%, corresponding to an increase in Pd particle size from 2 to 9 nm, resulted in a significant increase in the catalyst selectivity to the N-ethylcarbazole product. The consumption of octahydro-N-ethylcarbazole and tetrahydro-N-ethylcarbazole was much slower for the 0.5 wt.% and 0.7 wt.% catalysts. As seen in Fig. 6, no consumption of tetrahydro-N-ethylcarbazole was observed in the first 120 min of the reaction. However, complete conversion of the two intermediates, octahydro-N-ethylcarbazole and tetrahydro-N-ethylcarbazole, to N-ethylcarbazole was obtained within about 95 min over the 4 wt.% Pd/SiO_2 (Fig. 7). The selectivity to N-ethylcarbazole decreased with a further increase in the Pd loading to 5 wt.% and 10 wt.%, corresponding to Pd particle diameters of 13–15 nm (Fig. 8). These results are compared to the low selectivity observed over the Pd/SiO_2 prepared by calcination in air with a Pd particle size of 24 nm (Fig. 8), reported previously [8].

The measured consumption of the reactant dodecahydro-N-ethylcarbazole as a function of time was fitted to a 1st-order kinetic model, and the estimated rate constants are reported in Table 3. Initial turn-over frequencies (TOFs) with respect to the consumption of dodecahydro-N-ethylcarbazole were calculated using the estimated 1st-order rate constants and the initial concentration of reactant used in the experiments, as follows:

$$\mathrm{TOF} = \frac{k \cdot AW_{\mathrm{Pd}} \cdot C_{\mathrm{A0}}}{M_{\mathrm{Pd}} \cdot D} \quad (1)$$

where k is the 1st-order rate constant for dodecahydro-N-ethylcarbazole consumption (min^{-1} g_{cat}^{-1} lit), AW_{Pd} is the atomic mass of Pd ($g\ mol^{-1}$), C_{A0} is the reactant initial concentration ($mol\ cm^{-3}$), M_{Pd} is the Pd loading (wt.%) and D is the Pd dispersion (%). It is seen from Table 3 that the reaction rate constant based on catalyst concentration increased significantly from 0.0036 min^{-1} g_{cat}^{-1} lit to 0.0921 min^{-1} g_{cat}^{-1} lit as the Pd loading increased from 0.5 wt.% to 4 wt.%, and decreased to 0.0618 min^{-1} g_{cat}^{-1} lit with a further increase in Pd loading to 10 wt.%. The same trends were observed for the TOF of the reaction, where the 4 wt.% catalyst resulted in the highest TOF of 221.2 min^{-1} for the consumption of dodecahydro-N-ethylcarbazole. The catalysts with 0.5 wt.% and 0.7 wt.% Pd loading resulted in the lowest values of the reaction rate constants and TOFs. Fig. 9 plots the dodecahydro-N-ethylcarbazole dehydrogenation TOFs versus the Pd particle size for all the Pd/SiO_2 catalysts of the present study. From Fig. 9, it follows that the catalyst with a Pd particle size of about 9 nm, corresponding to the 4 wt.% Pd/SiO_2 catalyst, had the highest TOF. On the other hand, decreasing the particle size to about 2 nm with the 0.5 wt.% Pd catalyst resulted in a significant reduction in the TOF. Furthermore, an increase in the Pd particle size to about 12.5 nm with the 5 wt.% and 15 nm with the 10 wt.% catalysts, as well as the previously reported 24 nm with the 5 wt.% catalyst prepared by calcination in air [8,9], showed a decrease in the reactant consumption TOF.

Catalyst selectivity to N-ethylcarbazole at 50 % reactant conversion, as well as the selectivity after 1 h reaction at 443 K and 101 kPa over the different Pd/SiO_2 catalysts, is summarized in Table 4. At 50% conversion, a maximum selectivity of 15.3% to N-ethylcarbazole was obtained in 4 min over the 4 wt.% Pd/SiO_2. The selectivities at 50% reactant conversion, shown in Table 4, demonstrate that increasing the Pd loading from 0.5 wt.% to 4 wt.% and accordingly increasing the Pd metal particle diameter from 2 nm to 9 nm increased the observed selectivity to the com-

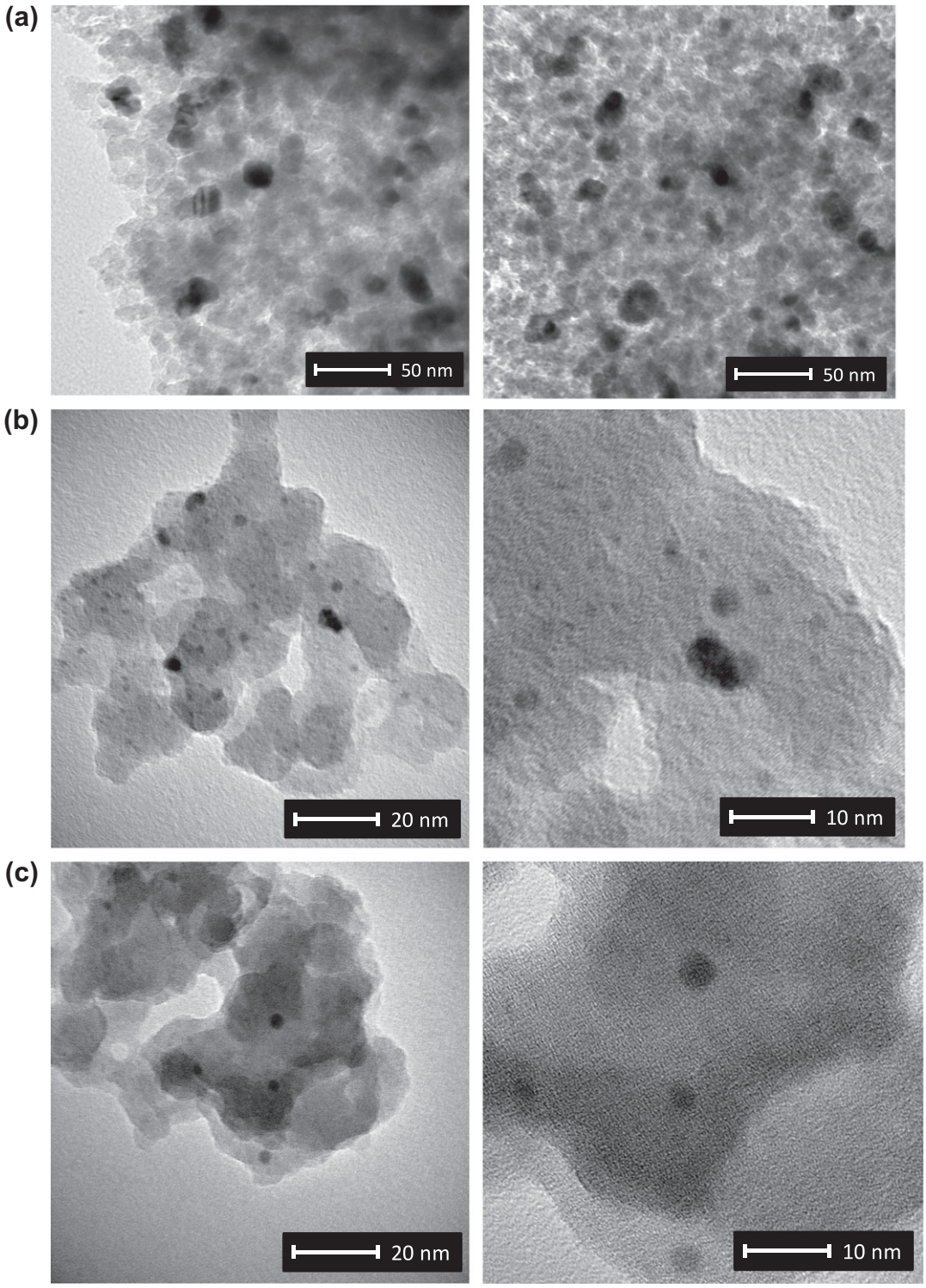

Fig. 5. Selected HRTEM images of reduced Pd/SiO_2 samples. (a) 10 wt.% Pd, (b) 4 wt.% Pd, and (c) 0.5 wt.% Pd. Samples were calcined in He flow at 773 K for 6 h prior to reduction in H_2 at 673 K for 1 h.

pletely dehydrogenated product, N-ethylcarbazole. With a further increase in Pd particle size, a decrease in the selectivity to N-ethylcarbazole was observed. The selectivity to N-ethylcarbazole decreased to 11.1% and 5.5% for the 5 wt.% and the 10 wt.% catalysts, respectively (Table 4). Complete conversion of the reactant was achieved in 22 min over the 4 wt.% catalyst, with 95% selectivity to N-ethylcarbazole during the first hour of reaction.

The H_2 recovery profile of the dehydrogenation of dodecahydro-N-ethylcarbazole at 443 K and 101 kPa over the 4 wt.% Pd/SiO_2 is compared to the 5 wt.% Pd/SiO_2 reported previously [8] in Fig. 10. The dramatic increase in the evolved H_2, observed using the 4 wt.% Pd/SiO_2 catalyst, is clear with the H_2 recovery completed within 96 min. Complete conversion of the reactant was obtained in only 22 min. Table 5 summarizes the H_2 recovery results

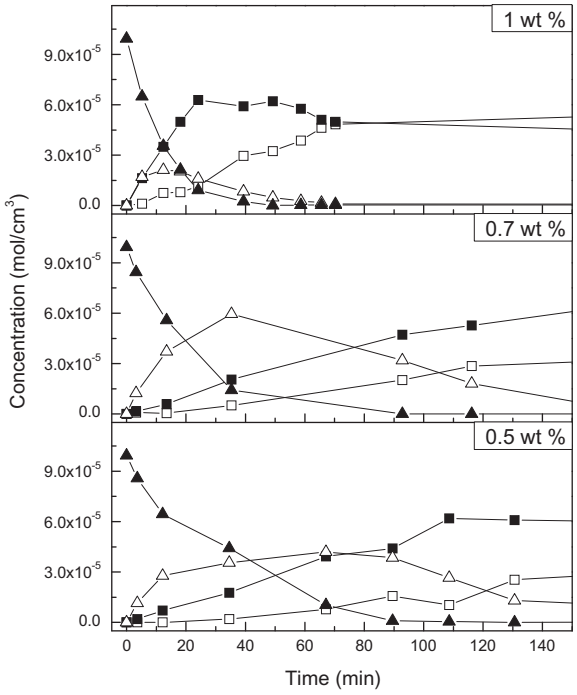

Fig. 6. Product distribution from dodecahydro-N-ethylcarbazole dehydrogenation at 443 K and 101 kPa over Pd/SiO_2 with Pd loading of 0.5, 0.7, and 1 wt.%; (▲), dodecahydro-N-ethylcarbazole, (Δ) octahydro-N-ethylcarbazole, (■) tetrahydro-, N-ethylcarbazole, and (□) N-ethylcarbazole.

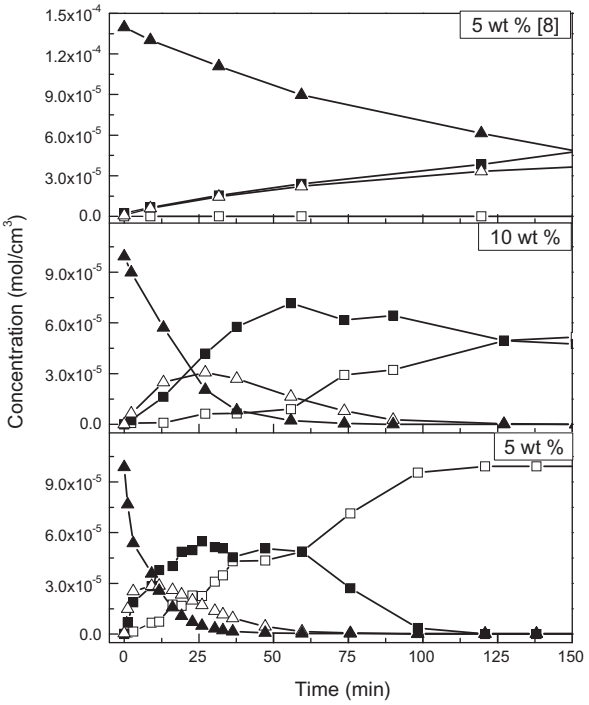

Fig. 8. Product distribution for dodecahydro-N-ethylcarbazole dehydrogenation at 443 K and 101 kPa over Pd/SiO_2 with Pd loading of 5, 10, and 5 wt.% (air calcined) [8]; (▲) dodecahydro-N-ethylcarbazole, (Δ) octahydro-N-ethylcarbazole, (■) tetrahydro-N-ethylcarbazole, and (□) N-ethylcarbazole.

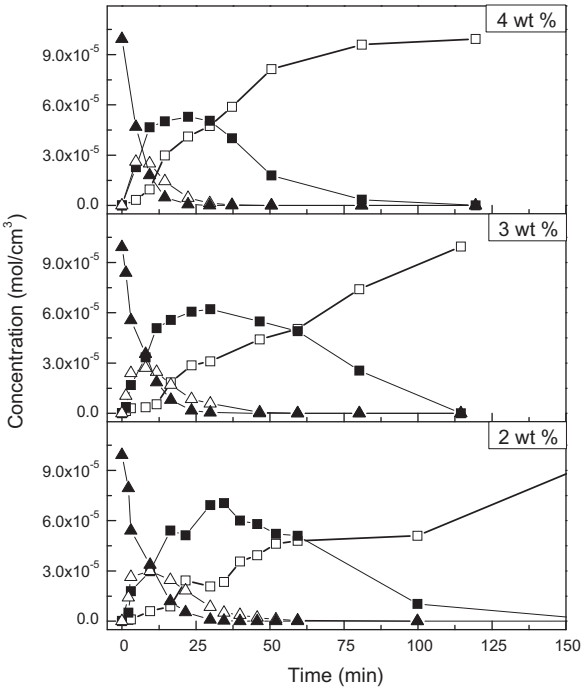

Fig. 7. Product distribution from dodecahydro-N-ethylcarbazole dehydrogenation at 443 K and 101 kPa over Pd/SiO_2 with Pd loading of 2, 3, and 4 wt.%; (▲), dodecahydro-N-ethylcarbazole, (△) octahydro-N-ethylcarbazole, (■) tetrahydro-, N-ethylcarbazole, (□) N-ethylcarbazole.

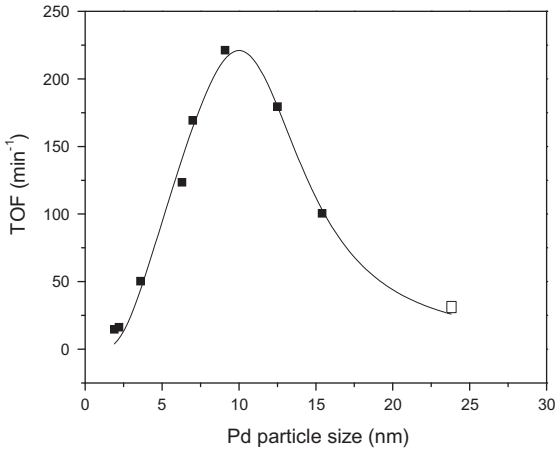

Fig. 9. TOFs for dodecahydro-N-ethylcarbazole dehydrogenation at 443 K and 101 kPa over Pd/SiO_2 catalyst with different Pd metal particle size. The open data point represents the TOF over the 5 wt.% Pd/SiO_2 reported by Sotoodeh et al. [8,9]. The solid line represents the data fit using Murzin's model given in Eq. (2) [45,46]. The fitted parameter values were $P_1 = 1.394 \pm 1.189$, $P_2 = 0.0020 \pm 0.0016$, $\gamma = 81.60 \pm 12.01$ and $\alpha = 0.124 \pm 0.030$, with $R^2 = 97.7\%$.

obtained for all of the Pd catalysts. Complete H_2 recovery, equal to the theoretical amount of 5.8 wt.%, was obtained in 1.6 h using the 4 wt.% Pd/SiO_2 catalyst. These results are excellent compared to the 17 h required for complete conversion reported previously over the 5 wt.% Pd/SiO_2 with 4.2% metal dispersion [8]. The results demonstrate that the 4 wt.% Pd/SiO_2 catalyst with average particle diameter of 9 nm and 11% Pd metal dispersion was the most active catalyst among those examined for the dehydrogenation of dodecahydro-N-ethylcarbazole.

3.3. DFT calculations

Fig. 11 illustrates the optimized adsorption geometries of dodecahydro-N-ethylcarbazole, octahydro-N-ethylcarbazole and

Table 3
First-order rate constants and turn-over frequencies (TOFs) for dehydrogenation of dodecahydro-N-ethylcarbazole at 443 K and 101 kPa over Pd/SiO_2 catalysts with different Pd loadings.

Pd loading (wt.%)	Rate constant[b] (min^{-1})	Rate constant [b] (min^{-1} g_{cat}^{-1} lit)	Initial concentration (mol cm^{3-1})	TOF [c] (min^{-1})
0.5	0.0457 ± 0.0033	0.0036	9.9350×10^{-5}	14.67
0.7	0.0535 ± 0.0023	0.0049	9.9350×10^{-5}	16.32
1	0.0935 ± 0.0022	0.0134	9.9350×10^{-5}	50.43
2	0.1496 ± 0.0048	0.0374	9.9272×10^{-5}	123.45
3	0.1668 ± 0.0047	0.0626	9.9260×10^{-5}	169.39
4	0.2148 ± 0.0082	0.0921	9.9350×10^{-5}	221.16
5	0.1139 ± 0.0015	0.0683	9.8764×10^{-5}	179.54
10	0.0618 ± 0.0034	0.0618	9.9350×10^{-5}	100.50
5[a]	0.0075 ± 0.0002	0.0045	1.3969×10^{-4}	31.85

[a] Reported previously by Sotoodeh et al. [8].
[b] With respect to dodecahydro-N-ethylcarbazole consumption.
[c] Molecule dodecahydro-N-ethylcarbazole. min^{-1} Pd surface $atom^{-1}$.

Table 4
Comparison of the selectivity to N-ethylcarbazole and the conversion of dodecahydro-N-ethylcarbazole at 443 K and 101 kPa over Pd/SiO_2 catalysts calcined in He.

Pd (wt.%)	Selectivity to N-ethylcarbazole at 50% reactant conversion (%)	Reaction time to obtain 50% conversion (min)	Selectivity to N-ethylcarbazole at 1 h (%)
0.5	3.1	27.9	8.8
0.7	3.0	17.0	14.2
1	4.7	9.5	39.0
2	9.0	5.0	48.3
3	9.5	4.7	50.8
4	15.3	3.8	94.8
5	11.1	5.5	49.6
10	5.5	16.1	17.9

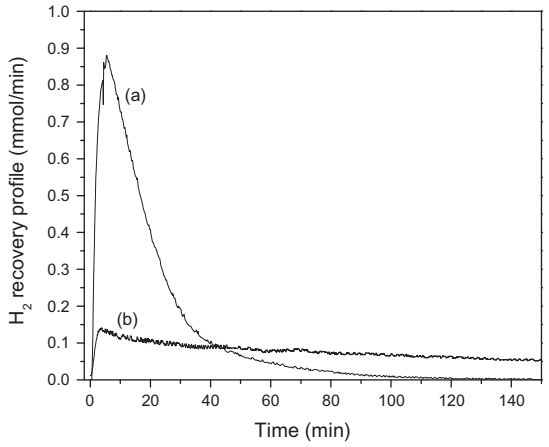

Fig. 10. H_2 recovery profile comparison for dodecahydro-N-ethylcarbazole dehydrogenation at 443 K and 101 kPa (a) over 4 wt.% Pd/SiO_2 prepared by calcination in He (b) over 5 wt.% Pd/SiO_2 calcined in air and reported previously, [8,9].

tetrahydro-N-ethylcarbazole on a Pd(1 1 1) surface. Atop adsorption of dodecahydro-N-ethylcarbazole through the two H atoms in the 5-membered ring adjacent to N heteroatom was favored. A calculated adsorption energy of −95.0 kJ/mol was obtained. The weakening of the C—H bonds was characterized by a significant increase in the two axial C—H bond distances, from 1.11 Å to about 1.16 Å. This suggests that dehydrogenation of dodecahydro-N-ethylcarbazole likely starts from the cleavage of the two axial C—H bonds in the 5-membered ring adjacent to the N heteroatom.

Table 5
H_2 recovery for the dehydrogenation of dodecahydro-N-ethylcarbazole at 443 K and 101 kPa over Pd/SiO_2 with different Pd loadings.

Pd loading (wt.%)	H_2 recovery[a] in 1 h (wt.%)	Final H_2 recovery (wt.%)
0.5	2.5	3.8 (6 h)[c]
0.7	3.1	4.4 (6 h)
1	3.3	5.2 (6 h)
2	4.7	5.8 (2.7 h)
3	4.8	5.8 (1.9 h)
4	5.4	5.8 (1.6 h)
5	4.7	5.8 (3 h)
10	4.0	5.8 (6 h)
5[b]	1.1	4.0 (17 h)

[a] Mass of H_2 released divided by the initial mass of dodecahydro-N-ethylcarbazole (theoretical H_2 recovery of dodecahydro-N-ethylcarbazole is 5.8 wt.%).
[b] Reported by Sotoodeh et al. [8,9].
[c] Experimental time to achieve the H_2 recovery reported.

Experimental data showed that dehydrogenation of dodecahydro-N-ethylcarbazole proceeded with removal of four H atoms from the 5-membered ring, resulting in production of octahydro-N-ethylcarbazole. Presumably, after the activation of the two axial C—H bonds, two more H atoms on the 5-membered ring are rapidly activated to produce octahydro-N-ethylcarbazole. The top view of Fig. 11a shows that the remaining H atoms on the 5-membered ring are in close proximity to the Pd surface atoms of the Pd(1 1 1) surface. The calculated adsorption energy of octahydro-N-ethylcarbazole (Fig. 11b) was −56.0 kJ/mol. Dehydrogenation of octahydro-N-ethylcarbazole was followed by removal of H atoms from one of the 6-membered rings to produce tetrahydro-N-ethylcarbazole (Fig. 11c). The adsorption energy of tetrahydro-N-ethylcarbazole was calculated as −117.5 kJ/mol.

The structure sensitivity of dodecahydro-N-ethylcarbazole dehydrogenation was also investigated by comparing the adsorption geometry of dodecahydro-N-ethylcarbazole over a Pd(1 1 0) surface with that of Pd(1 1 1). Fig. 12 illustrates the optimized geometry of the dodecahydro-N-ethylcarbazole adsorbed on top of the Pd(1 1 0) surface. The molecule locates on the surface so that the interaction of the two H atoms adjacent to N, increases (Fig. 12a). The calculated adsorption energy on the Pd(1 1 0) surface was −83.2 kJ/mol. The C—H bond distance increase from 1.11 Å to about 1.16 Å was observed for the adsorption of the molecule over the Pd(1 1 0) surface (Fig. 12b) which was the same as that obtained on the Pd(1 1 1) surface. No other C—H bond distance change was identified. Fig. 12c shows the top view of the adsorption geometry of dodecahydro-N-ethylcarbazole. The two H atoms adjacent to the N heteroatom are in atop positions, but note that the remaining H atoms of the 5-membered ring are located above Pd atoms in the second layer of the Pd(1 1 0) surface, making H removal on this surface less likely than on the Pd(1 1 1) surface.

4. Discussion

4.1. Catalyst properties

The water peaks observed during temperature-programmed calcination of silica gel in He or air at 373–473 K (Figs. 2 and 3) are ascribed to the removal of surface and micropore-absorbed water [34,35], whereas the water loss at higher temperature (773 K) is ascribed to water loss from hydrogen-bonded silanol groups. The latter assignment follows work by Li et al. [35] who reported an infrared (IR) analysis of silica gel as temperature was increased to 773 K. The intensity of a band at 3650 cm^{-1}, related to hydrogen-bonded silanol groups, decreased with increased temperature, whereas a band at 3720 cm^{-1}, related to free silanol

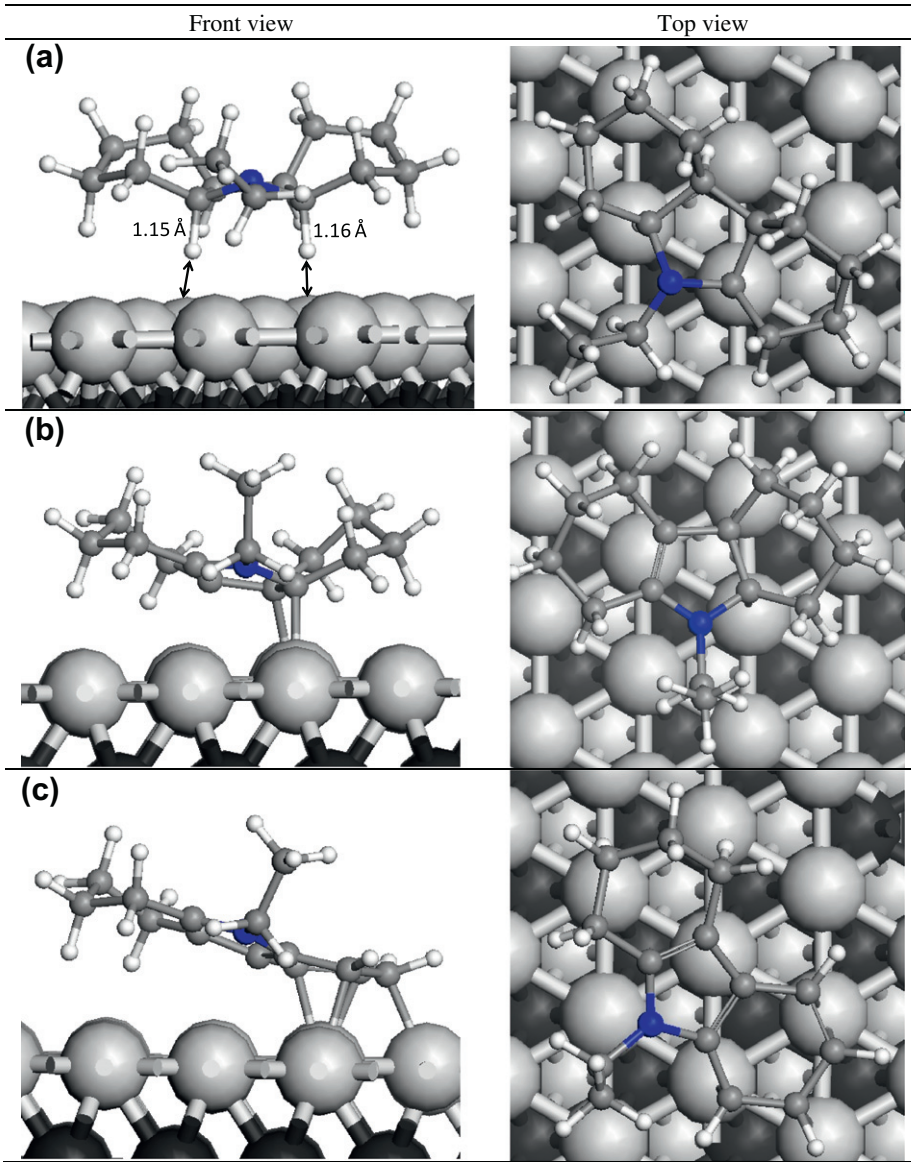

Fig. 11. Optimized adsorption geometries of (a) dodecahydro-N-ethylcarbazole showing the interaction of the two H atoms with the nearest Pd surface atoms, (b) octahydro-N-ethylcarbazole and (c) tetrahydro-N-ethylcarbazole over Pd(1 1 1) surface. Blue: N, white: H, gray: C, light gray: first layer Pd atoms, and black: second layer Pd atoms.

groups, increased slightly due to the conversion of some of the hydrogen-bonded silanol groups absorbing at 3650 cm^{-1} into free silanol groups absorbing at 3720 cm^{-1} plus water.

The preparation of Pd catalysts supported on Al_2O_3 [36] and SiO_2 [37] using $PdCl_2$ as the precursor has been well studied. $PdCl_4^{2-}$ results when $PdCl_2$ is dissolved in acidic solutions [38] and Contescu et al. [36] have shown that the $PdCl_4^{2-}$ is partially hydrolyzed in solution to yield $PdCl_2(H_2O)^-$ and $PdCl_2(H_2O)_2$ species. These species adsorb electrostatically onto acidified alumina. In the present work, the impregnation was conducted at low pH (<2), below the isoelectric point of silica, so that a similar electrostatic adsorption on $SiOH_2^+$ can be expected. When the impregnated alumina was dried in air at 385 K for 3 h, Contescu et al. [36] demonstrated that $PdCl_4$ (70–75%) and $PdCl_xO_y$(25–30%) were generated as a consequence of dehydration of the hydrolyzed $PdCl_4^{2-}$ and reaction with atmospheric oxygen. Calcination at higher temperature (up to 925 K) in air resulted in further oxidation of the precursor, yielding PdO_x (35–45%) and an increased amount of $PdCl_xO_y$(55–65%). The presence of $Pd_xO_yCl_z$ species on Pd/Al_2O_3 catalysts has been identified in other studies [24]. Vilarrasa-Garcıa et al. [39] detected the formation of metallic Pd and palladium oxychloride by XPS of activated carbons impregnated with $PdCl_2$ and dried in He at 393 K for 6 h. Palladium oxychloride species were also identified by XPS of air-calcined Pd catalysts before reduction in H_2 by Normand et al. [40]. The TPR data of Fig. 3 are consistent with these same transformations of the precursor impregnated on silica. Accordingly, H_2O was released at ~460 K and a second peak was observed at 773 K (Fig. 3). The two H_2O peaks likely correspond to the water removal from the silica support as discussed earlier, as well as dehydration of two different hydrolyzed Pd species, as identified by Contescu et al. [36]. Of most significance, however, is the fact that no HCl (nor any other chlorinated products) was observed during the air drying and calcination of the catalyst precursors. This implies that the Pd precursors did not lose Cl during drying and calcination in air, and the catalyst precursor, following drying, must be mostly PdO_xCl_y species, such as the $PdClO_4$ and $PdCl_2O_3$ identified on Pd/alumina precursors following similar drying and calcination steps [36]. Furthermore, there was no color

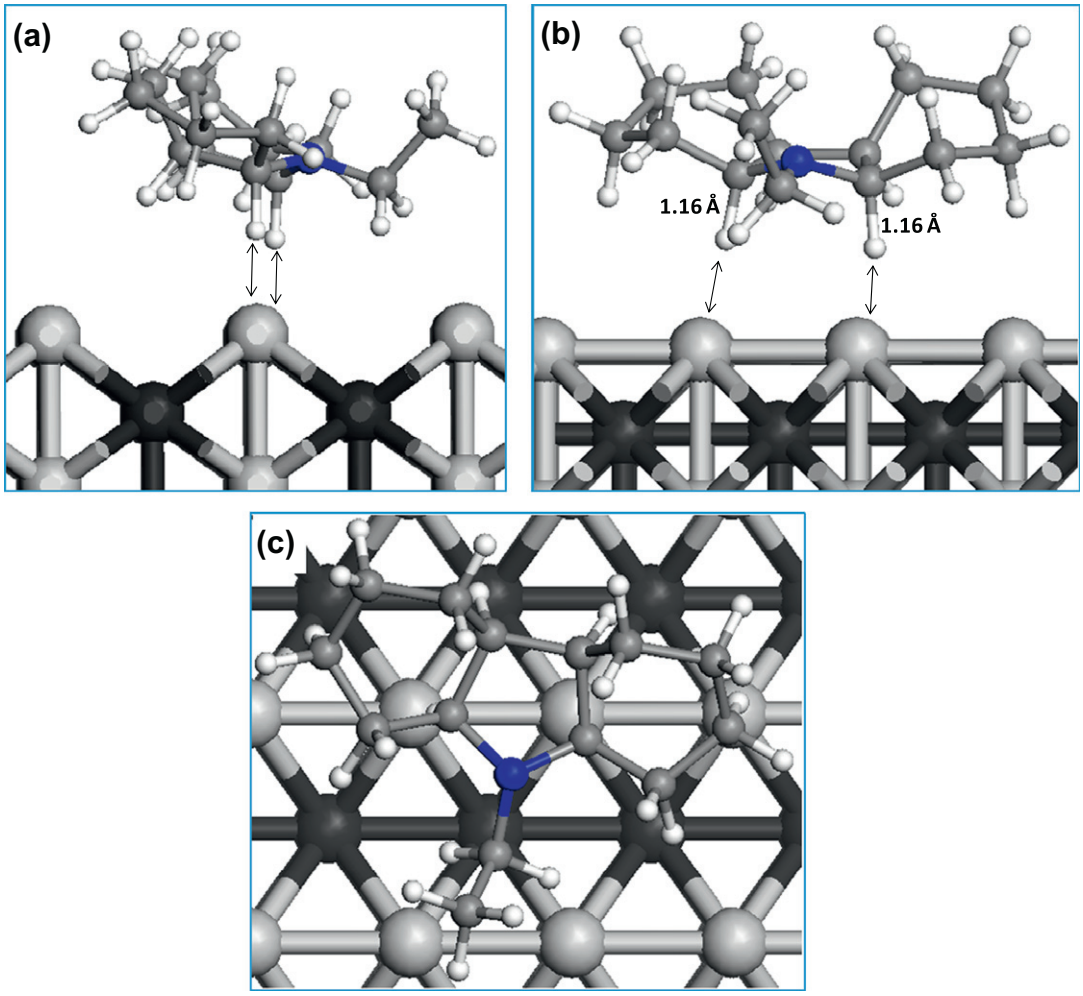

Fig. 12. Optimized adsorption geometry of dodecahydro-N-ethylcarbazole over Pd(1 1 0) surface; (a) side view showing the interaction of the two H atoms with the first layer Pd surface, (b) front view showing the C—H bond distances increase from 1.10 Å in vacuum to 1.16 Å upon approaching the surface, and (c) top view. The molecule moves so that the two C—H bonds adjacent to N heteroatom are at atop positions over the nearest Pd atoms. Blue: N, white: H, gray: C, light gray: first layer Pd atoms, and black: second layer Pd atoms.

change observed following calcination of the Pd/SiO_2 catalyst precursor in air, indicative of PdO_xCl_y species rather than PdO_x.

In contrast, Fig. 2 shows that when the impregnated silica was dried and calcined in inert He, a significant amount of HCl was detected, suggesting that reactions of the type $PdCl_2 + H_2O \rightarrow PdO + 2\,HCl$ occurred, rather than the oxidations that occurred in air to yield PdO_xCl_y. In this instance, the samples recovered after calcination were black, indicative of PdO_x species. The TPR profile also shows that only one peak was observed for the HCl evolution, and this occurred at a temperature very similar to the second peak temperature for water evolution (~773 K). The profile is consistent with the dehydration of the hydrolyzed Pd precursors as already mentioned and indicates that the removal of the Cl likely only occurs from $PdCl_2$ or $PdCl_4^{2-}$ species, rather than hydrolyzed Pd species.

Following calcination, the precursors were flushed in H_2 at room temperature before being reduced according to the TPR protocol already described. HCl and H_2O were both evolved from the catalysts during the hydrogen flush and the TPR, confirming the reduction of the precursors to Pd^0 during both processes (Figs. 2 and 3). The reduction of $PdCl_2$ at room temperature has been previously reported [41,42]. Although the reduction profiles for the He and air-calcined samples were very similar, for both the flush and the TPR, the sample calcined in He evolved more HCl, indicative of the easier reduction of $PdCl_2$ and PdO_x species on the He-calcined sample than the reduction of PdO_xCl_y species present on the air-calcined sample [36].

The stoichiometry for CO adsorption on Pd has been reported to depend on the Pd cluster size [29]. The differences in Pd particle size observed in Table 1 between the CO TPD and the HTREM results may be a consequence of a change in the CO:Pd adsorption stoichiometry as the Pd particle size increased. As reported in Table 1, catalyst dispersion was significantly increased for the catalysts prepared by calcination in He, compared to the catalyst prepared by wet impregnation and calcination in air [8,9]. The effect of pre-treatment on Pd catalyst dispersion has been reported previously by Zou et al. [37] where an increase in Pd dispersion was observed by calcination in a noble gas instead of O_2. The lower dispersion in the latter case was attributed to the competitive interaction between Pd and the oxygen in the support versus Pd and the gas phase oxygen, which resulted in a partial weakening of the metal-support interaction and agglomeration of the Pd. In the present work, the improved dispersion is more likely a consequence of the different precursors that result from calcination in air (PdO_xCl_y) versus He (PdO_x). The Pd oxychloride is known to be more difficult to reduce than the PdO_x [36] and the data of Figs. 2 and 3 show that the peak reduction temperature was about ~40 K higher for the air-calcined sample than the He-calcined sample. During the calcination process in He, both Cl and H_2O

are lost from the Pd precursor, and this likely results in a strong interaction between the Pd and the O of the SiO_2 support that anchors the Pd to the support. Consequently, during TPR, the Pd remains well dispersed. In the case of the air-dried sample however, because of the formation of PdO_xCl_y species that will reduce the interaction of Pd with the SiO_2, agglomeration of the PdO_xCl_y can occur, resulting in significantly lower dispersion of the air-calcined sample compared to the He-calcined sample. Furthermore, the PdO_xCl_y has been identified as providing nucleation sites for Pd crystallite growth [36], and the presence of PdO_xCl_y species in the air-calcined samples likely contributes to a reduced dispersion as well.

4.2. Catalyst activity and selectivity

From Fig. 9 and Table 4, it is seen that the 4 wt.% Pd/SiO_2 catalyst, with a Pd particle diameter of about 9 nm, resulted in a maximum in the dodecahydro-N-ethylcarbazole dehydrogenation TOF and a maximum in selectivity to the completely dehydrogenated product N-ethylcarbazole. The N-ethylcarbazole selectivity over the 4 wt.% Pd/SiO_2 catalyst was 15.3% at 50% reactant conversion and 95% after 1 h of reaction, significantly higher than that obtained for the other catalysts of Table 4. Complete conversion of the reactant was obtained in 22 min over the 4 wt.% Pd/SiO_2 catalyst, which is significantly shorter than the 17-h reaction time reported for dodecahydro-N-ethylcarbazole dehydrogenation at 443 K and 101 kPa over the 5 wt.% Pd/SiO_2 catalyst calcined in air [8,9]. In the present work, the complete H_2 recovery from dodecahydro-N-ethylcarbazole obtained over the 4 wt.% Pd/SiO_2 catalyst after 1.6 h at 443 K shows the significantly superior activity of the Pd/SiO_2 catalysts prepared by calcination in He rather than air.

The results reported herein are significant for hydrogen recovery applications, since the dehydrogenation reactions had previously been reported to be very slow with no selectivity to the completely dehydrogenated product, N-ethylcarbazole. Wang et al. [10] reported Ir complexes to be active for the dehydrogenation of dodecahydro-N-ethylcarbazole. Complete conversion occurred after 48 h at 473 K, but dehydrogenation to the fully unsaturated product N-ethylcarbazole did not occur and octahydro-N-ethylcarbazole and tetrahydro-N-ethylcarbazole were reported to be the only observed products. Crawford et al. [15] and Hindle et al. [43] reported that the dehydrogenation of tetrahydrocarbazole at 413 K and 101 kPa proceeded to 81% conversion over a 5 wt.% Pd/Al_2O_3 catalyst in 27 h, with an initial reaction rate of 10 mM min^{-1} g_{cat}^{-1}, in reasonable agreement with the initial rate of 17 mM min^{-1} g_{cat}^{-1} reported by the authors [8] over the 5 wt.% Pd/SiO_2 at 413 K and 101 kPa. Although 100% selectivity to the completely dehydrogenated product carbazole was obtained, product inhibition was shown to slow the reaction rate significantly. Decalin, another hydrogen storage candidate, was dehydrogenated over a Pt/C catalyst by Loutfy et al. [33] in a batch-type membrane reactor at temperatures of 533–593 K. Conversions below 85% were reported after 2.2 h. Conversions >95% were obtained within 1.5 h at 553 K by Hodoshima et al. [30]. However, these reported reaction temperatures (>535 K) are too high and impractical for hydrogen recovery for transport applications.

The dependence of the dodecahydro-N-ethylcarbazole dehydrogenation TOF and selectivity to N-ethylcarbazole on Pd particle size, clearly demonstrated in the present work, suggests that the dehydrogenation reaction is structure sensitive. Pd particle size likely plays an important role in providing an adequate ensemble of catalytic sites for adsorption of the large dodecahydro-N-ethylcarbazole molecule and the other dehydrogenation intermediates. The maximum in TOF with particle size observed in the present work has also been observed in other reaction systems. For example, Binder et al. [44] reported a maximum in the ethene hydrogenation TOF over Pd/TiO_2 catalysts at atmospheric pressure and 293 K, with the maximum occurring for a catalyst with a Pd particle size of 3 nm. Bezemer et al. [45] also reported a maximum in CO hydrogenation TOF over a series of Co catalysts, with the maximum occurring for a Co particle size of about 3 nm. Murzin [46,47] has shown that the maximum in TOF can be accounted for by an analysis of the kinetic consequences of the different reactivities of edges and terraces present on the metal catalyst and the dependence of the fraction of edges on the cluster or particle size. Accordingly, for both two-step reaction mechanisms and Langmuir–Hinshelwood kinetics, the TOF can be written as [46,47]:

$$\mathrm{TOF} = \frac{P_1 e^{(1-\alpha)\gamma/d_{cluster}}}{1 + P_2 e^{\gamma/d_{cluster}}} \tag{2}$$

where P_1 and P_2 are combinations of individual reaction frequencies, α is the Polanyi parameter, γ is the parameter accounting for the differences in Gibbs free energy of adsorption on terraces and edges and $d_{cluster}$ is the cluster diameter. The same equation will apply to the dehydrogenation TOF of dodecahydro-N-ethylcarbazole, and Fig. 9 shows the standard nonlinear least-squares fit of the data from the present study applied to Eq. (2). The estimated parameter values are reported in Fig. 9, and the maximum in TOF at a particle size of about 9 nm is well explained by Murzin's model. The Polanyi parameter obtained from the data fit was somewhat lower than the 0.5 often observed in heterogeneous catalytic reaction [46,47]. Furthermore, the difference in the Gibbs free energy of adsorption on terraces versus edges is suggested to be significantly larger (300 kJ/mol) than that reported for ethene hydrogenation [46].

Previous DFT studies reported by Crawford et al. [15] showed that tetrahydrocarbazole adsorbs on the Pd(1 1 1) surface through its aromatic ring aligned parallel to the surface with the aliphatic ring at 30° to the surface. This suggests that for octahydro-N-ethylcarbazole and tetrahydro-N-ethylcarbazole a large surface with several Pd atoms will be required to remove H atoms from the molecules. The low TOF for the conversion of reactant (Fig. 9) and low N-ethylcarbazole selectivity obtained over the highly dispersed catalysts (0.5, 0.7, and 1 wt.%) (Table 4) can be explained by the need for a large ensemble of Pd surface atoms required for adsorption of dodecahydro-N-ethylcarbazole and its dehydrogenation products.

Results from the DFT calculations of the present work are also in support of the structure sensitivity of dodecahydro-N-ethylcarbazole dehydrogenation. The DFT calculations showed that the dodecahydro-N-ethylcarbazole adsorbed parallel to the Pd(1 1 1) surface through several Pd surface atoms, a requirement for a structure-sensitive reaction. The DFT calculations also showed that the reaction was initiated by activation of the H atoms associated with the 5-membered ring of dodecahydro-N-ethylcarbazole. Experimental results were in agreement with these calculations in that octahydro-N-ethylcarbazole was identified as a primary product of the dehydrogenation, followed by stepwise H removal from one of the 6-membered rings to produce tetrahydro-N-ethylcarbazole. Cui et al. [2] reported that incorporation of an N heteroatom in the 5-membered ring greatly lowers the enthalpy of dehydrogenation of that ring for 1-methyloctahydroindole. However, the nitrogen raises the enthalpy of dehydrogenation of the 6-membered ring, so that dehydrogenation is expected to occur at the 5-membered ring first with subsequent dehydrogenation of the 6-membered ring. Both the experimental results and the DFT data of the present work are in agreement with these observations.

The structure sensitivity of the dehydrogenation reaction of dodecahydro-N-ethylcarbazole is also reflected in the adsorption geometry calculated by DFT for the molecule on the Pd(1 1 0) surface. The molecule adsorbs on the surface such that the two H

atoms adjacent to the N heteroatom interact with the Pd surface in a similar manner to that observed on Pd(1 1 1). However, because of the less-packed structure of the Pd(1 1 0) surface compared to the Pd(1 1 1) surface, the interaction between Pd and the remaining H atoms in the 5-membered ring is not possible. These H atoms are located above Pd atoms of the second layer of the Pd(1 1 0) surface (shown in Fig. 12a in black), and the distance between the H and Pd atoms is such that there is no interaction. Hence, to form octahydro-N-ethylcarbazole on the Pd(1 1 0) surface would require additional desorption and re-adsorption steps that are not required on the Pd(1 1 1) surface. These observations also point to the fact that the dehydrogenation of dodecahydro-N-ethylcarbazole is structure dependent.

5. Conclusion

Dodecahydro-N-ethylcarbazole dehydrogenation is shown to be structure sensitive over Pd/SiO_2 catalysts. With a Pd particle size of 9 nm, complete hydrogen recovery was achieved in less than 2 h at 443 K and 101 kPa. DFT and experimental results show that dehydrogenation of dodecahydro-N-ethylcarbazole starts from the 5-membered ring to produce octahydro-N-ethylcarbazole as the primary intermediate. The adsorption of dodecahydro-N-ethylcarbazole involves several Pd surface atoms and the adsorption energy is dependent on the surface structure, results that support the observed structure sensitivity of the reaction.

Acknowledgments

Funding for the present study from the Natural Sciences and Engineering Research Council of Canada is gratefully acknowledged. The authors would also like to acknowledge the Bio-Imaging Facility in the Department of Botany at the University of British Columbia for the high-resolution transmission electron microscopy (HRTEM) measurements.

References

[1] S. Satyapal, J. Petrovic, C. Read, G. Thomas, G. Ordaz, Catal. Today 120 (2007) 246–256.
[2] Y. Cui, S. Kwok, A. Bucholtz, B. Davis, R. Whitney, P. Jessop, New J. Chem. 32 (2008) 1027–1037.
[3] G. Cacciola, N. Giordano, G. Restuccia, Int. J. Hydrogen Energy 9 (1984) 411–419.
[4] D. Klvana, A. Touzani, J. Chaouki, G. Belanger, Int. J. Hydrogen Energy 16 (1991) 55–60.
[5] U. Eberle, M. Felderhoff, F. Schueth, Angew. Chem. Int. Ed. 48 (2009) 6608–6630.
[6] G. Pez, A. Scott, A. Cooper, H. Cheng, US Patent 7 101 530 B2, 2006.
[7] A. Moores, M. Poyatos, Y. Luo, R. Crabtree, New J. Chem. 30 (2006) 1675–1678.
[8] F. Sotoodeh, L. Zhao, K.J. Smith, Appl. Catal. A Gen. 362 (2009) 155–162.
[9] F. Sotoodeh, K.J. Smith, Ind. Eng. Chem. 49 (2010) 1018–1026.
[10] Z. Wang, I. Tonks, J. Belli, C. Jensen, J Organomet. Chem. 694 (2009) 2854–2857.
[11] A. Benedetti, G. Fagherazzi, F. Pinna, G. Rampazzo, M. Selva, G. Strukul, Catal. Lett. 10 (1991) 2115.
[12] D. Suh, T. Park, S. Ihm, Ind. Eng. Chem. 31 (1992) 1849.
[13] G. Neri, M. Musolino, C. Milone, D. Pietropaolo, S. Galvagno, Appl. Catal. A Gen. 208 (2001) 307–316.
[14] J. Kuhn, W. Huang, C. Tsung, Y. Zhang, G. Somorjai, J. Am. Chem. Soc. 130 (2008) 14026–14027.
[15] P. Crawford, R. Burch, C. Hardacre, K. Hindle, P. Hu, B. Kalirai, D.W. Rooney, J. Phys. Chem. 111 (2007) 6434–6439.
[16] Y. Lu, H. Zhang, Y. Xu, B. Song, H. Li, S. N Bao, P. He, Appl. Surf. Sci. 253 (2006) 2025–2030.
[17] A. Vargas, T. Bürgi, A. Baiker, J Catal. 226 (2004) 69–82.
[18] J.R. Regalbuto, Catalyst Preparation: Science and Engineering, Taylor and Francis Group, LLC, 2007.
[19] M. Ohara, Y. Kim, S. Yanagisawa, Y. Morikawa, M. Kawai, Phys. Rev. Lett. 136104 (2008) 100.
[20] W. Dou, J. Chem. Phys. 244711 (2008) 128.
[21] A. Becke, Phys. Rev. A 38 (1988) 3098.
[22] B. Hammer, L. B Hansen, J.K. Norskov, J. Phys. Rev. B 59 (1999) 7413.
[23] J. Perdew, K. Burke, M. Ernzerhof, Phys. Rev. Lett. 77 (1996) 3865.
[24] N. Babu, N. Lingaiah, R. Gopinath, P. Reddy, P. Prasad, J. Phys. Chem. C 111 (2007) 6447–6453.
[25] C. Amairia, S. Fessi, A. Ghorbel, A. Rives, J Mol. Catal. A Chem. 332 (2010) 25–31.
[26] M. Gurrath, T. Kuretzky, H. Boehm, L. Okhlopkova, A. Lisitsyn, V. Likholobov, Carbon 38 (2000) 1241–1255.
[27] J. Bakker, A. Geert van der Neut, M. Kreutzer, J. Moulijn, F. Kapteijn, J Catal. 274 (2010) 176–191.
[28] M. Myyrylainen, T. Rantala, Catal. Today 100 (2005) 413–417.
[29] R. Hicks, Q. Yen, A. Bell, J. Catal. 89 (1984) 498–510.
[30] S. Hodoshima, H. Arai, S. Takaiwa, Y. Saito, Intl. J. Hydrogen Energy 28 (2003) 1255–1262.
[31] O. Stull, E. Westrum, G. Sinke, The Chemical Thermodynamics of Organic Compounds, John Wiley and Sons Inc., New York, 1969.
[32] E. Newson, T. Truong, P. Hottinger, F. Roth, T. Schucan, 12th World Hydrogen Energy Conference, 21–25 June 1998, Buenos Aires, Argentina, pp. 935–942.
[33] R. Loutfy, E. Veksler, Int. Hydrogen Energy Forum, 11–15 September 2000, Munich. Germany, pp. 335–340.
[34] R. Iler, The Chemistry of Silica, John Wiley and Sons, New York, 1979.
[35] Z. Li, Q. Zhao, C. Liu, Y. Wang, J. Cent. South Univ. Technol. 5 (1998) 31–34.
[36] C. Contescu, D. Macovei, C. Craiu, C. Teodorescu, J.A. Schwarz, Langmuir 11 (1995) 2031.
[37] W. Zou, R. Gonzalez, Cataly. Lett. 12 (73) (1992) 73–86.
[38] T. Mang, H. Knozinger, J. Hightower, W. Delgass, E. Iglesia, A. Bell, in: Proc. 11th Int. Congress on Catal., Baltimore, 1996.
[39] E. Vilarrasa-Garcıa, A. Infantes-Molina, R. Moreno-Tost, E. Rodrıguez-Castellon, A. Jimenez-Lopez, Jr.C. L Cavalcante, D.C.S. Azevedo, Energy Fuels 24 (2010) 3436–3442.
[40] F.L. Normand, J. Barrault, R. Breault, L. Hilaire, A. Kiennemann, J. Phys. Chem. 95 (1991) 257.
[41] J. Murthy, S. Chandra Shekar, A. Padmasri, A. Venugopal, V. Kumar, B.M. Nagaraja, V. Shashikala, B.D. Raju, P. Kanta Rao, K.S. Rama Rao, Catal. Commun. 5 (2005) 161167.
[42] W. Jozwiak, T. Maniecki, Thermochim. Acta 435 (2005) 151–161.
[43] K. Hindle, R. Burch, P. Crawford, C. Hardacre, P. Hu, B. Kalirai, D.W. Rooney, J. Catal. 251 (2007) 338–344.
[44] A. Binder, M. Seipenbusch, M. Muhler, G. Kasper, J. Catal. 268 (2009) 150–155.
[45] G.L. Bezemer, J.H. Bitter, H.P.C.E. Kuipers, H. Oosterbeek, J.E. Holewijn, X. Xu, F. Kapteijn, A.J. van Dillen, K.P. de Jong, J. Am. Chem. Soc. 128 (2006) 3956.
[46] D.Y. Murzin, J. Catal. 276 (2010) 85–91.
[47] D.Y. Murzin, J Mol. Catal. A Chem. 315 (2010) 226–230.